(4)

OFFICE OF NAVAL RESEARCH

Contract N00014-87-K-0494

R&T Code 400X027YIP

Technical Report No. 2

Scanning Tunneling Microscopy of Platinum Films on Mica. Evolution of Topography and Crystallinity During Film Growth

by

E. R. Scott, H. S. White, and D. J. McClure

Prepared for Publication in the

Journal of Physical Chemistry

University of Minnesota
Department of Chemical Engineering and Materials Science
Minneapolis, MN 55455

Dec. 5, 1988

SECURITY CLASSIFICATION OF THIS PAGE

REPORT DOCUMENTATION PAGE

1a. REPORT SECURITY CLASSIFICATION Unclassified	1b. RESTRICTIVE MARKINGS
2a. SECURITY CLASSIFICATION AUTHORITY	3. DISTRIBUTION/AVAILABILITY OF REPORT
2b. DECLASSIFICATION/DOWNGRADING SCHEDULE	Unclassified/Unlimited
4. PERFORMING ORGANIZATION REPORT NUMBER(S) ONR Technical Report 2	5. MONITORING ORGANIZATION REPORT NUMBER(S)
6a. NAME OF PERFORMING ORGANIZATION Dept of Chemical Engineering and Materials Science 6b. OFFICE SYMBOL (If applicable) Code 1113	7a. NAME OF MONITORING ORGANIZATION Office of Naval Research
6c. ADDRESS (City, State, and ZIP Code) University of Minnesota Minneapolis, MN 55455	7b. ADDRESS (City, State, and ZIP Code) 800 North Quincy Street Arlington, VA 22217
8a. NAME OF FUNDING/SPONSORING ORGANIZATION Office of Naval Research 8b. OFFICE SYMBOL (If applicable)	9. PROCUREMENT INSTRUMENT IDENTIFICATION NUMBER Contract No. N00014-87-K-0494
8c. ADDRESS (City, State, and ZIP Code) 800 North Quincy Street Arlington, VA 22217-5000	10. SOURCE OF FUNDING NUMBERS PROGRAM ELEMENT NO. / PROJECT NO. / TASK NO. / WORK UNIT ACCESSION NO.

11. TITLE (Include Security Classification)
Scanning Tunneling Microscopy of Platinum Films on Mica. Evolution of Topography and Crystallinity During Film Growth

12. PERSONAL AUTHOR(S)
E.R. Scott, H.S. White, D.J. McClure

13a. TYPE OF REPORT	13b. TIME COVERED	14. DATE OF REPORT (Year, Month, Day)	15. PAGE COUNT
Technical	FROM _____ TO _____	December 5, 1988	

16. SUPPLEMENTARY NOTATION

17 COSATI CODES			18. SUBJECT TERMS (Continue on reverse if necessary and identify by block number)
FIELD	GROUP	SUB-GROUP	r.f. sputter deposition; ~~ultra-smooth Pt films~~ Platinum films, (mgm)

19. ABSTRACT (Continue on reverse if necessary and identify by block number)

Scanning tunneling microscopy (STM) was used to characterize the topography and crystallinity of Pt films deposited on mica by r.f. sputtering. Three stages of film growth were identified by STM for films of thicknesses, d, between 20 and 1500Å. Images of ultrathin Pt films, d<50Å, show a rippled topography with no resolvable features associated with ordered crystalline growth. At intermediate coverages, 60<d<200Å, 50-150Å diameter crystalline grains are resolved by STM. The shape and size of these grains are nearly identical to that observed by transmission electron microscopy. Large, flat grains (diameter ≈ (approx.) 1000Å) with a nearly atomically smooth topography are observed for films of thickness ≥ 500Å. STM images of Pt films immersed under water an in mineral oil, and images of mobile surface contaminants are also reported.

20. DISTRIBUTION/AVAILABILITY OF ABSTRACT	21. ABSTRACT SECURITY CLASSIFICATION
☒ UNCLASSIFIED/UNLIMITED ☐ SAME AS RPT ☐ DTIC USERS	Unclassified
22a. NAME OF RESPONSIBLE INDIVIDUAL Henry S. White	22b. TELEPHONE (Include Area Code) (612) 625-6995 22c. OFFICE SYMBOL

DD FORM 1473, 84 MAR 83 APR edition may be used until exhausted. All other editions are obsolete.

SECURITY CLASSIFICATION OF THIS PAGE

Scanning Tunneling Microscopy of Platinum Films on Mica. Evolution of Topography and Crystallinity During Film Growth

Erik R. Scott, Henry S. White*
Department of Chemical Engineering and Materials Science
University of Minnesota
Minneapolis, MN 55455

and

D. J. McClure
3M Corporate Research
Process Technologies Laboratory
St. Paul, MN 55144

Abstract. Scanning tunneling microscopy (STM) was used to characterize the topography and crystallinity of Pt films deposited on mica by r.f. sputtering. Three stages of film growth were identified by STM for films of thicknesses, d, between 20 and 1500Å. Images of ultrathin Pt films, d< 50Å, show a rippled topography with no resolvable features associated with ordered crystalline growth. At intermediate coverages, 60 < d < 200Å, 50-150Å diameter crystalline grains are resolved by STM. The shape and size of these grains are nearly identical to that observed by transmission electron microscopy. Large, flat grains (diameter ≈ 1000Å) with a nearly atomically smooth topography are observed for films of thickness ≥ 500Å. STM images of Pt films immersed under water and in mineral oil, and images of "mobile" surface contaminants are also reported.

* To whom correspondence should be addressed.

Introduction. The development of scanning tunneling microscopy (STM)[1,2] has provided a powerful technique for monitoring interfacial structure resulting from the deposition of molecular and atomic species on a conducting substrate. Providing vertical resolution on the order of tenths of angstroms and lateral resolution in the angstrom range, STM is capable of measuring surface structures with dimensions ranging from the atomic scale to thousands of angstroms. These capabilities appear particularly promising for studies of metal and semiconductor thin film growth where the structure and topography continually evolve from nucleation until a thick, bulk-like overlayer is deposited.

In the present report, we have used STM to characterize the evolution of surface topography and crystallinity of Pt films deposited on mica by r.f. sputtering[3,4]. The motivation for this research is two-fold: First, the structure and properties of ultrathin metal films on mica is of interest in ongoing electrochemical studies by ourselves and by others. Pt and Au films are used in the fabrication of electrodes of nanoscopic dimensions[5,6], requiring the formation of molecularly thin (<100Å) continuous films. Au films deposited on mica have been employed as ultra-smooth substrates for deposition and subsequent imaging of compact films of aliphatic organic monomers[7]. Mica/Pt structures have recently been used by ourselves[8] and by Bard and coworkers[9,10] in conjunction with surface forces microbalance[11] techniques. In this latter application, the force or current is measured between two Pt film electrodes closely separated by a thin electrolytic layer (0 - 1000Å) . The topography of these films and the presence of surface contaminants, both resolvable by STM, are key factors in the analysis of these measurements.

Second, the mechanism by which noble metal atoms and clusters condense on an relatively inert substrate, such as mica, to form a continuous film is not well understood. A detailed STM investigation of highly ordered crystalline Au films of thickness 500-4800Å, thermally evaporated onto mica, has been reported by Chidsey, et. al.[7] However, thin film properties and structure strongly depend on specific chemical and physical interactions between the substrate and the material being deposited, and on the deposition technique and

parameters, e.g., temperature, deposition rate, etc. Markedly differing STM and electron microscopy images of Pt films deposited on mica have been recently reported by ourselves and by other laboratories. For instance, Miranda et. al. observed a rippled and relatively rough topography on 50Å thick Pt films[12]. Fan and Bard recently reported a nearly atomically smooth topography on thick (1.8 μm) films on mica[13]. Our laboratory reported observations of well defined 50-75Å wide Pt crystallites in 60Å thick films using transmission electron microscopy (TEM)[8]. Crystallites of these dimensions apparently were not observed in either of the previous STM studies. In the present work, we have used STM to demonstrate that all of the above mentioned observations are, in fact, representative of the structure of Pt on mica that occur during different stages of film growth.

Experimental. Pt was r.f. sputtered at a rate of 4Å/min. onto freshly cleaved muscovite mica (Unimica Corp., NY.) at room temperature. Details of the deposition technique have been described previously[3]. Since mica is electrically insulating and is cleaved to yield molecularly smooth regions (up to several cm^2), it is presumed that all surface features observed in STM images are associated with the metal films, and not the underlying substrate. Films of 40, 60, 100, 200, 500, 1000, and 1500Å thickness were imaged using a Digital Instruments, Inc. Nanoscope II scanning tunneling microscope. The STM scans a tunneling tip across a sample at a tip/sample separation of a few angstroms. A negative feedback loop controls the tip height as it raster scans across the surface. In this report, the scan direction of the tip is parallel to the X-axis indicated on each figure. At high feedback gain, a "constant current" image is obtained by plotting the tip height vs. the tip position on the surface. Conversely, by lowering the gain in the feedback loop a "constant height" image is obtained by plotting the logarithm of the tunneling current vs. tip position. Scan rates varied from 9-34 lines/sec. Tunneling currents ranged from 0.2-3.0 nA. In-air

images were made with a sample-tip bias of +50 mV, while in-water images were taken with biases ranging from 25-1000 mV.

Tunneling tips were cut from 0.01" wire. Tungsten (Alfa Chemical) was used when imaging in air, while Pt-13%Rh (Omega Engineering) was used in water. Sharp asperities on the tips, capable of routinely obtaining atomic resolution of cleaved pyrolytic graphite, were obtained by cutting either type of wire with a diagonal wire cutter. For the samples studied in this work, these tips were found to perform equally as well as those obtained by electropolishing. The tips extended ca. 3mm from a stainless steel tip holder. In-water imaging was performed with the sample immersed under ca. 1mm of water. No insulation was applied to the tips. Samples were imaged in 18 mega-ohm water purified using a Labconco (Kansas City, MI) Water Prodigy system. Tunneling under mineral oil was done by placing a single drop of mineral oil (Alfa Chemical) on the sample.

Post-processing of images involved removing high frequency noise by replacing each data point with the weighted average of itself and its eight nearest neighbors. In some cases, it was necessary to subtract the average Z-value of a line scan to reduce the effects of low frequency (<10 Hz) noise.

Results and Discussion. The discussion of results obtained from STM imaging of Pt films are separated into two sections. First, we present a series of STM images of Pt films of thickness between 40 and 1500Å. This sequence shows the evolution of the film topography beginning with a 40Å thick conductive layer. We then present selected images of Pt films immersed in H_2O and oil. Similar "in-situ" imaging of platinum and pyrolytic graphite in aqueous electrolytes has been recently demonstrated by several laboratories[13,14,15,16,17,18,19,20]. Our particular interest in this technique is related to contamination of Pt films used in surface forces microbalance.

STM is uniquely capable of measuring features associated with film growth over a wide range of dimensions. However, several factors affect the reproducibility of the

images. Due to surface heterogeneity, and the fact that it is essentially impossible to scan the same area of a sample on two different occasions, no two images taken at different sessions will be identical. Surface impurities adsorbed on the sample can also cause an image to change with time (*vide infra*). Each of the images presented below for a particular film thickness is representative of qualitative structure and topography observed on several samples of the same thickness.

Dependence of Topography and Crystallinity on Film Thickness. Figs. 1(a) - (f) show in-air STM images over a 400 x 400Å area of 40, 60, 100, 500, 1000, 1500 Å thick Pt films. Each film was prepared by the same deposition procedure and at a constant deposition rate (4Å/min.). The thicknesses of Pt films less than 100Å thick were verified by ellipsometric measurements using reported optical constants (η = 2.26; k = 4.66 at 632.8 nm). These measurements yield values within 10% of the expected mass average thickness. Quoted thicknesses for films greater than 200Å are based on the calibration of the constant deposition rate by ellipsometry. The images in Fig. 1 were obtained at a tunneling current set-point of 0.5 nA and a sample-tip bias of 50mV. All images in Fig. 1 were recorded in constant current mode.

Images of 40Å thick films (Fig. 1a) show randomly sized features which are aligned $\approx 60^{o}$ to the direction of scanning (X-axis). The alignment of features in Fig. 1a is similar but not as pronounced as that previously observed in STM images of 50Å Pt films thermally evaporated onto mica and attributed to columnar growth.[12] STM images of 60Å films, Fig. 1b, show a marked change in topography relative to that observed on the 40Å thick films. In this image, and in constant current images of films of thickness up to 200Å, the film topography is characterized by rounded grains with a 10-20Å vertical separation between the crest of each mound and the lowest point lying along the grain boundaries. The grain diameter increases slightly from 50-75Å for 60Å thick films, to 120-150Å for 200Å thick films. (Fig. 4a shows the topography of a 100Å thick film prepared by the

same procedure, but immersed in H_2O. The diameter of the mounds (80-100Å) at this thickness is intermediate between that observed on the 60 and 200Å films).

The ordered features seen in the 60, 100, and 200Å thick films are no longer observed in the images when the film thickness is increased to 500Å, Fig. 1d. Instead, the topography is characterized by shallow hills with lateral dimensions ranging up to 300Å. Smaller features (5-10Å vertical heights) are superimposed on the broader hills, but the more regular and textured topography apparent in thinner films is noticeable absent. The diminishment of features with small lateral dimensions continues as the film thickness is further increased. For instance, images of 1000Å and 1500Å thick films, Figs. 1e and 1f, show large irregularly shaped crystalline grains which grow larger with increasing film thickness. However the films are extremely smooth over small areas. For example, the RMS roughness (prior to filtering of noise) on a 200 x 200Å area of the image in Fig. 1f. is measured to be ≈ 5Å.

The larger grains on the 1000 and 15000Å thick films are more apparent in images taken over a wider area, Fig. 2. The diameters of the grains observed in 5000 x 5000Å scans, Fig. 2, range from 300-1500Å. The average vertical step between neighboring grains is about 100Å, and the grains themselves appear much flatter than the rounded mounds observed on thinner films (Figs. 1b, 1c and 4).

Discussion of Film Growth. The series of STM images of Pt films, Figs. 1 & 2, as a function of thickness allows qualitative arguments to be presented concerning the mechanism of film growth. Based on these observations, we propose that at least three stages of growth occur (Scheme I) *following* deposition of mass quantities of Pt that correspond to a continuous and electrically conductive film.

Previous transmission electron micrographs[8] of 20Å thin films and the STM images of 40Å thick Pt films, Fig. 1a, suggest that the initial deposition of Pt results in a film composed of very small crystallites or metal clusters. Individual crystal facets have not yet

been resolved by STM or TEM, but the electron diffraction pattern of 20Å films, previously reported by our laboratories[8], shows a continuous ring pattern corresponding to an randomly oriented polycrystalline Pt layer. We believe that sputter deposition of 40Å of Pt reproducibly yields a continuous film with physical properties similar to bulk polycrystalline Pt. Evidence substantiating this includes: (1) coincidence of d.c. electrical conductivity and optical constants of the 40Å films with bulk Pt; (2) electron diffraction studies; (3) and electrochemical behavior of the films in 0.1 M H_2SO_4 similar to that observed using bulk polycrytalline Pt electrodes[8]. STM images of 40Å thick films, although showing local roughness, are qualitatively simila at different locations on the film suggesting that the metal film is free of microscopic voids exposing bare mica.

When the film thickness is increased to a value between 60 and 200Å, regularly spaced rounded mounds are observed, suggesting a film composed of hemispherical metal grains. These rounded features are inconsistent with previous TEM images of 60Å thick films, Fig. 3a, which show flat crystals separated by well defined boundaries. We believe that the *roundness* of the grains observed by STM may possibly be an artifact of the imaging process. When the feedback gain controlling the tip-sample distance is adjusted to a very small value and the tunneling current is plotted on the Z-axis, (e.g., constant height mode), a qualitatively different image is obtained. For example, Fig. 3b shows an image of a 60Å film obtained using low gain feedback. The image has been tilted 60Å towards the page so that the observation view is more similar to that of the TEM image in the Fig. 3a. The STM and TEM images are strikingly similar, both in the size and shape of the grains, and definition of crystalline facets.. The well defined grains have been observed in STM images of 60-200Å thick films, although the features are most well resolved for 60Å thick samples. No features of similar structure or dimensions have been observed in images for 40Å thick films, in agreement with the previous TEM studies, or in images of films of thickness greater than 200Å.

The differences in STM images obtained in the constant current and constant height modes is not presently understood. In imaging polycrystalline films with grains sizes of 50Å, the STM tip diameter is at least of the same order of magnitude as the surface features themselves. If boundaries between features are too deep or narrow, the tip will not likely be able to probe into them accurately, losing resolution. There may also be inherent differences in the tunneling current along grains boundaries causing the tip to overshoot to different degrees in the two scanning modes. Regardless, the uniqueness of the rounded mounds (observed in high feedback mode) or flat angular crystallites (observed in low feedback mode) to film thicknesses between 60 and 200Å suggests a coalescing of small crystallites in thinner films (40Å or less) to yield a a film composed of larger grains, Scheme Ib.

Between 200 and 500Å , the small grain structure is replaced by films with a topography that is much smoother over small areas, but which contains crystalline grains with much larger dimensions. This abrupt transformation in topography resembles the transition in structure observed between 40 and 60Å but on a much larger scale. Increasing the thickness to 1000 and 1500Å, Figs. 1e, 1f, and 2, yields well defined grains with a similar mosaic structure. We believe that these large grains must result from either (1) preferential lateral growth of a few of the smaller underlying grains (see dotted structure in part (c) of Scheme I) or (2) coalescing of the 50-75Å diameter grains.

In relation to ongoing applications of these films in electrochemical studies, STM imaging has demonstrated that films as thin as 40Å can be prepared that are microscopically continuous and of relatively uniform thickness. The measured 10-15Å roughness of 40Å thick films is slightly larger that our preliminary 10Å estimate based on the hard-wall contact distance between two 40Å Pt films brought together in the surface forces microbalance. For microscopically rough surfaces, the hard wall contact distance provides a rough estimate of the distance that the two surfaces can be pushed together before contacting. Although nearly atomically smooth facets are observed on films of 100-

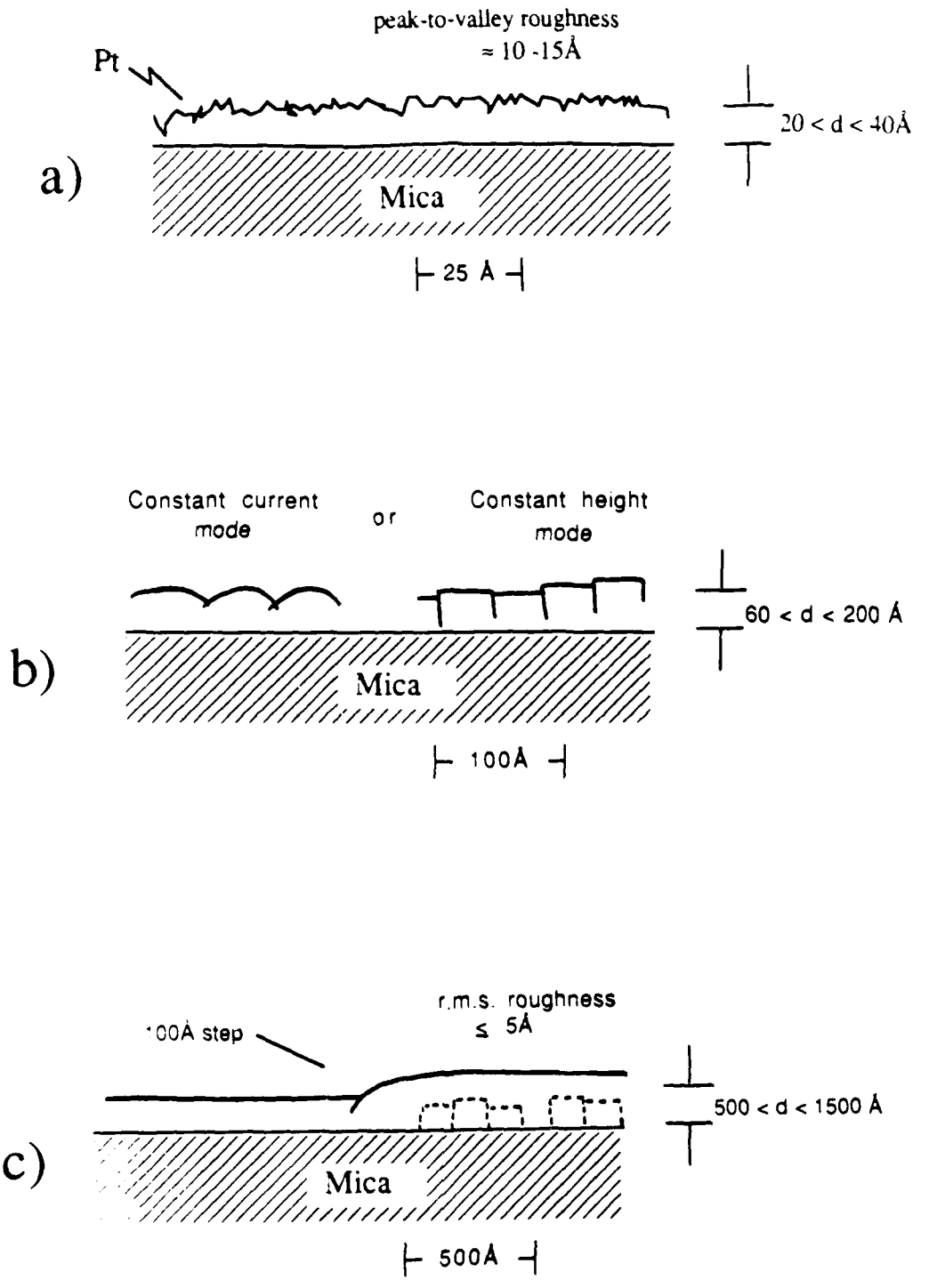

Scheme I. Representation of the topography and crystallinity of Pt films r.f. sputtered on mica as a function of film thickness. The indicated dimensions of various surface features are based on STM and TEM imaging.

1500Å thickness, the larger vertical separation between neighboring grains (typically 100Å) would probably give a much larger apparent roughness in similar surface forces measurements.

Mobile surface Contaminants. Adsorbed impurities on the samples were sometimes found to appear during in-air scanning. Although it is known that the metal surfaces are readily contaminated by H_2O and organics following exposure to air, we have obtained indirect evidence from surface force measurements for the presence of relatively thick (20-40Å) contaminant layers on Pt. The STM images presented below demonstrate the presence of mobile "fluid-like" clusters that may be responsible for these previous observations.

The impurities usually take the form of a solid particle or a thin (≈20Å), semifluid film, coating most or all of the region being scanned, typically 500x500Å. In the latter case, features associated with the semifluid film continually change shape during scanning while prominent Pt features protruding through the impurity film remain stable. The fluid film can often be "swept" off of the scanned area by increasing the linear scan dimensions by an order of magnitude for a few seconds, and then reducing the scan size back down to the area of interest.

Images of mobile impurities were found to be captured most easily while tunneling under a bulk fluid layer. Figs. 4a and b show constant current images of the same area of a *clean* 100Å sample under H_2O taken at 0.2nA, with sample/tip biases of 25 and 1000mV, respectively. The average peak to valley depth of the 100Å diameter grains is 20Å, which is commensurate with in-air images of the 60 and 200Å films. The image taken at 1000mV appears to lose some of the vertical detail of that taken at 25mV, however the differences between the two images are slight. This fact demonstrates that if moderate measures are taken to maintain water purity, images will not be affected by faradaic currents at moderate to large biases. Although the literature contains references to tunneling under electrolytic

solutions using tips which are insulated from the electrolyte except for at the very end, this measure is not necessary for imaging in deionized water.

The images in Figs. 5a and b. were taken of the same area of a 100Å thick Pt film , two minutes apart from one another. The prominent feature in Fig. 5a completely disappears in Fig. 5b. The rapid, complete disappearance suggests that a solid particle, loosely adsorbed onto the Pt was brushed aside by the tip during the intervening time between the capturing of the two images. Another class of impurity is observed in the lower center regions of Figs 6a . and b. These images show the change in shape of a large, fluid-like cluster in the lower center of a 100Å thick sample after an interval of 15 minutes. The small ripples seen on the flat region of the Pt specimen are the crystallites described earlier, poorly resolved due to the large scan dimensions. Close examination of the position of the large cluster with respect to fixed landmark features of the Pt shows no noticeable bulk migration of the cluster, however the cluster does become about 50% narrower in the X direction. Since this narrowing is not accompanied by any apparent elongation in the Y or Z directions, the tip's role seems to have been to cause molecules to be drawn off of the cluster and enter into the mineral oil.

Summary. STM images presented here, in conjunction with previous TEM studies, provide a detailed characterization of the evolution of the structure of Pt films during growth. The topography and crystallinity of these films is strongly dependent on film thickness. Nucleation of the film results in a uniform and continuous polycrystalline film composed of small (<15Å) Pt particles. At a thickness of ca. 50Å a more ordered film topography is observed with crystalline grain sizes on the order of 50-150Å. Increasing the film thickness to 500 - 1500Å results in a topography characterized by large flat grains with a nearly atomically smooth topography. STM images of polycrystalline films composed of small grains (~50Å diameter) are strongly dependent on the feedback gain used to control the tip-surface separation.

Acknowledgement. Financial support was provided in part by the Department of Energy/Office of Basic Energy Science and by Medtronics, Inc. (Minneapolis). STM facilities are supported by the Center for Interfacial Engineering with funding from NSF Engineering Research Centers Program (CDR 8721551) and industrial sponsors. H.S.W. gratefully acknowledges support provided by the Office of Naval Research Young Investigator Program.

Figure Captions

Fig. 1. STM images of r.f. sputtered deposited Pt films on mica as a function of the film thickness. (Constant current mode; current = 3.0nA; sample-tip bias = 50 mV)

Fig. 2. Large area STM images of (top) 1000Å and (bottom) 1500Å thick Pt films. (Constant current mode; current = 0.5nA; sample-tip bias = 50mV)

Fig. 3. (a) TEM image (from ref. 8) and (b) STM image of a 60Å Pt film. (Constant height mode; current = 3.3nA; sample-tip bias = 30mV)

Fig. 4. (a) STM images of a 100Å thick Pt film immersed under H_20 (tunneling current = 0.2nA; sample-tip bias = 25mV). (b) same region scanned at a sample-tip bias of 1000 mV.

Figure 5. (a) STM image of a large solid particle on a 100Å thick Pt film immersed in mineral oil. The particle appears in the upper left region of the top image. The lower image (b) shows the identical area after 2 minutes of scanning.

Fig. 6. (a) STM image of a 4000Å wide fluid-like cluster on a 100Å Pt film. After 15 min. of scanning, (b), the size of the cluster is reduced to 2500Å.

References.

1. Binning, G.; Rohrer, H.; *Helv. Phys. Acta*, **1982**, 55, 726.

2. Binnig, G.; Rohrer, H.; Gerber, Ch.; Weibel, E.; *Appl. Phys. Lett*, **1982**, 40, 178.

3. Maeda, M.; White, H.S.; McClure, D. J.; *J. Electroanal. Chem.*, **1986**, 200, 383.

4. Liu, H.-Y.; Fan, F.-R.; Bard, A. J.; *J. Electrochem. Soc.*, **1985**, 132, 2666.

5. Morris, R., Franta, D., White, H.S., *J. Phys. Chem.*, **1987**, 91, 3559.

6. Wehmeyer, K. R.; Deakin, M.R.; Wightman, R.M., *Anal. Chem.*, **1985**, 57, 1913.

7. Chidsey, C.E.D.; Loiacono, D.N.; Sleator, T., Nakahara, S.;*Surf. Sci*, **1988**, 200, 45

8. Smith, C.P.; Maeda, M.; Atanasoska, Lj.; White, H.S.; McClure, D. J.; **J. Phys. Chem.**, **1988**, 92, 199.

9. Lee, C.-W.; Bard, A.J., *J. Electrochem. Soc.*, **1988**, 135, 1599.

10. Fan, F.-R., Bard, A. J.; *J. Am. Chem. Soc.*, **1987**, 109, 6262.

11. Israelachvili, J. N.; Tabor, D.; *Proc. R. Soc. London A.*, **1972**, 331, 19.

12. Miranda, R.; Garcia, N.; Baro, A. M.; Garcia, R.; Pena, J. L.; Rohrer, H.; *Appl. Phys. Lett.*; **1985**, 47, 367.

13. Fan, F.-R.; Bard, A. J.; *Anal. Chem.*, **1988**, 60, 751.

14. Liu, H. Y.; Fan, F.-R.; Lin, C. W.; Bard, A. J.; *J. Am. Chem. Soc.*, **1986**, 108, 3838.

15. Itaya, K.; Tomita, E.; *Surf. Sci.*, **1988**, 201, L507.

16. Sonnenfeld, R.; Hansma, P. K.; *Science*, **1986**, 232, 211.

17. Schneir, J.; Sonnenfeld, R.; Hansma, P. K.; Tersoff, J.; *Phys. Rev. B.*, **1986**, 34, 4979.

18. Drake, B.; Sonnenfeld, R.; Scheir, J.; Hansma, P. K.; *Surf. Sci.*, **1987**, 181, 92.

19. Sonnenfeld, R.; Schardt, B.C.; *Appl. Phys. Lett.*, **1986**, 49, 1172.

20 Gewirth, A.A.; Bard, A.J.; *J. Phys. Chem.*, **1988**, 92, 5563.

a) 40 Å

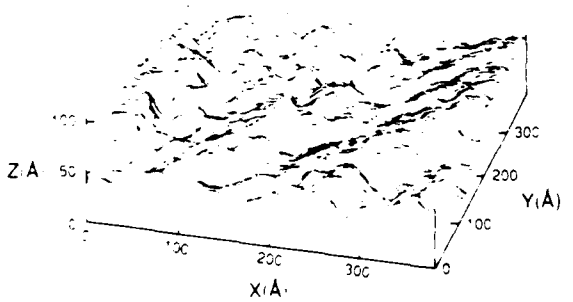

b) 60 Å

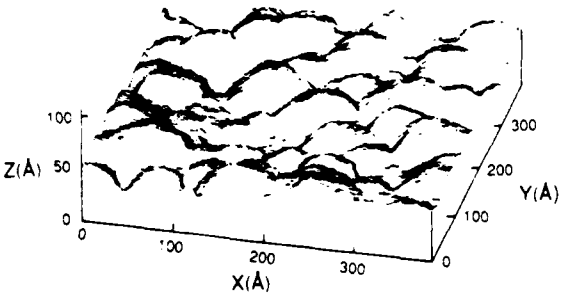

c) 200 Å

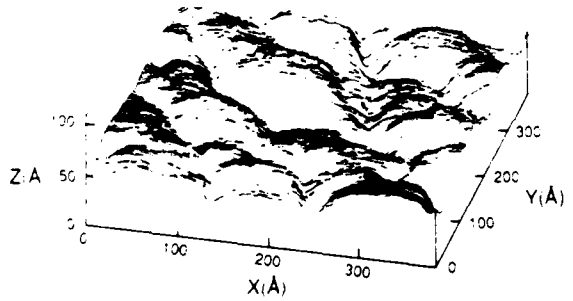

d) 500 Å

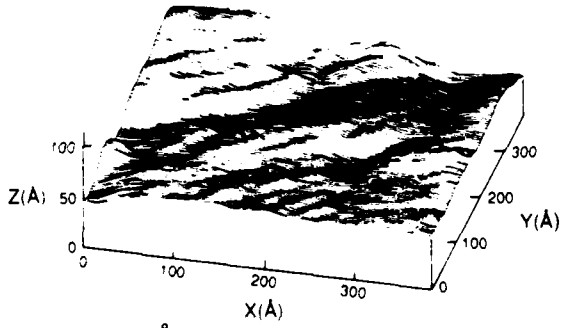

e) 1000 Å

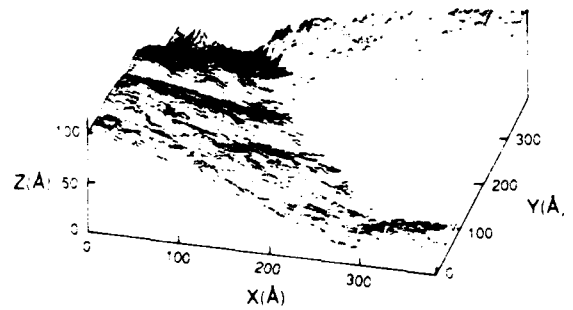

f) 1500 Å

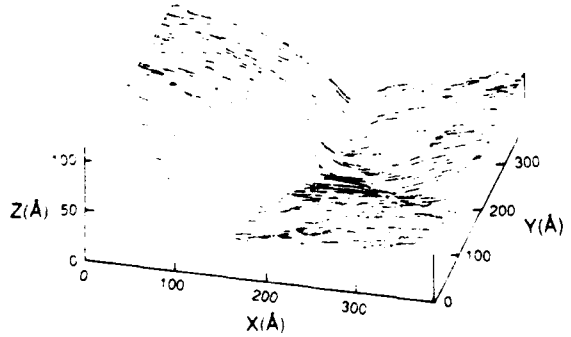

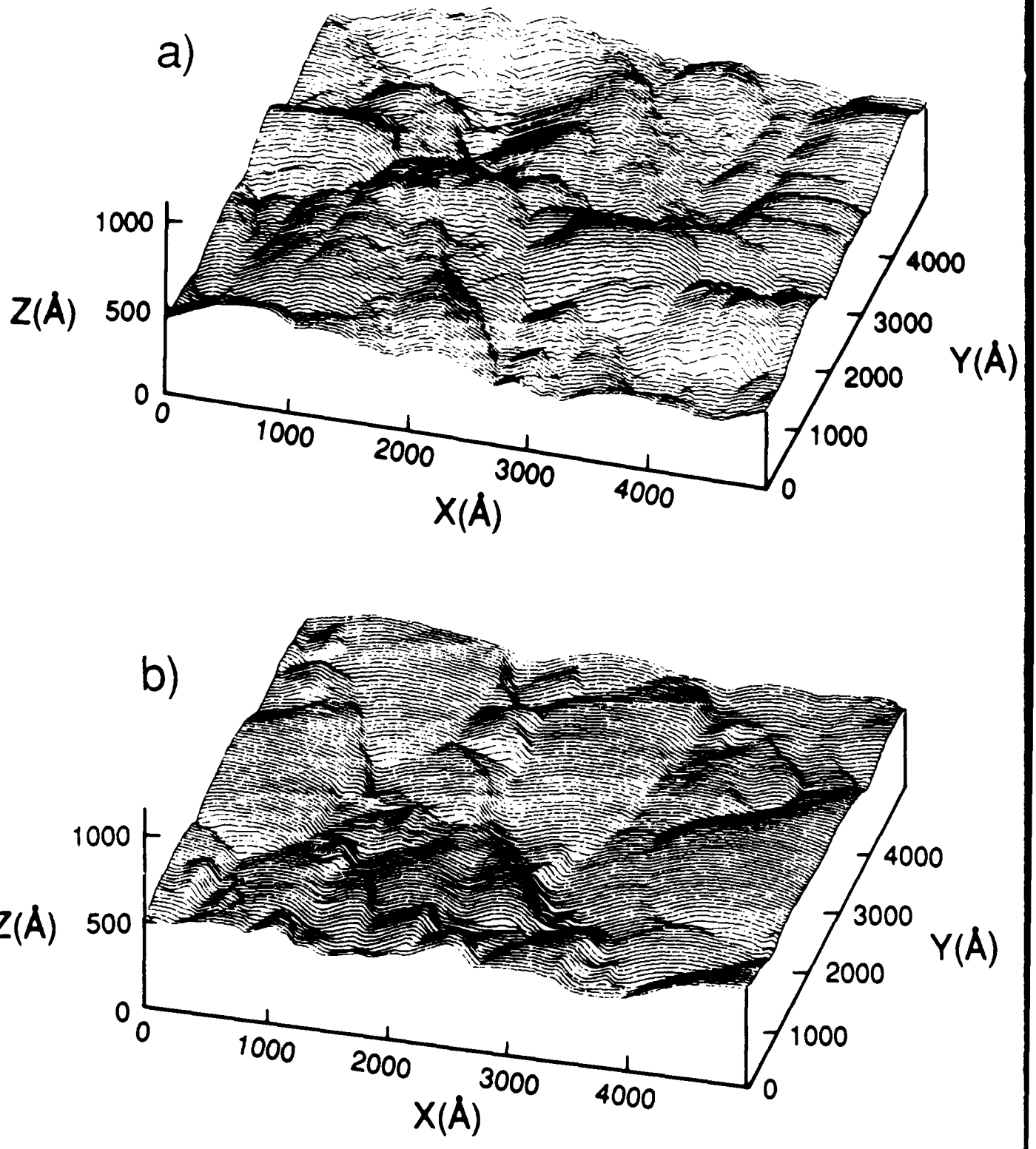
a)
1000
Z(Å)
500
0
0
1000
2000
3000
4000
X(Å)
4000
3000
2000
1000
0
Y(Å)
b)
1000
Z(Å)
500
0
0
1000
2000
3000
4000
X(Å)
4000
3000
2000
1000
0
Y(Å)

a)

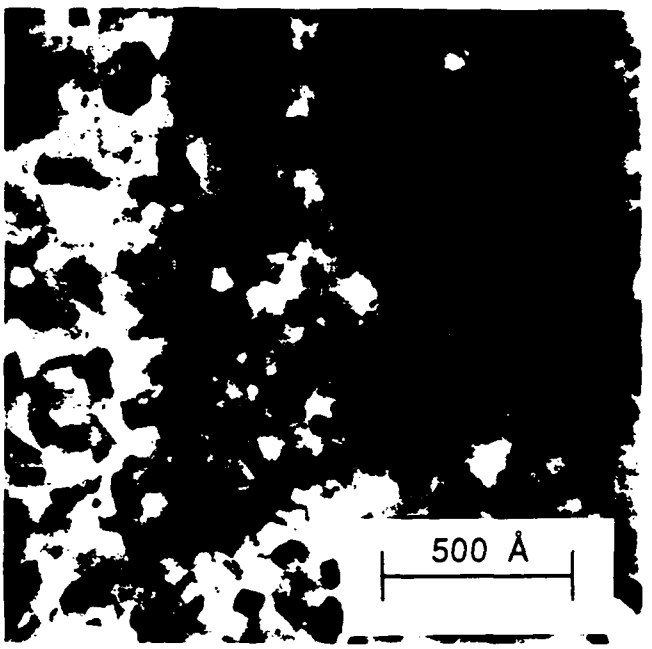

b)

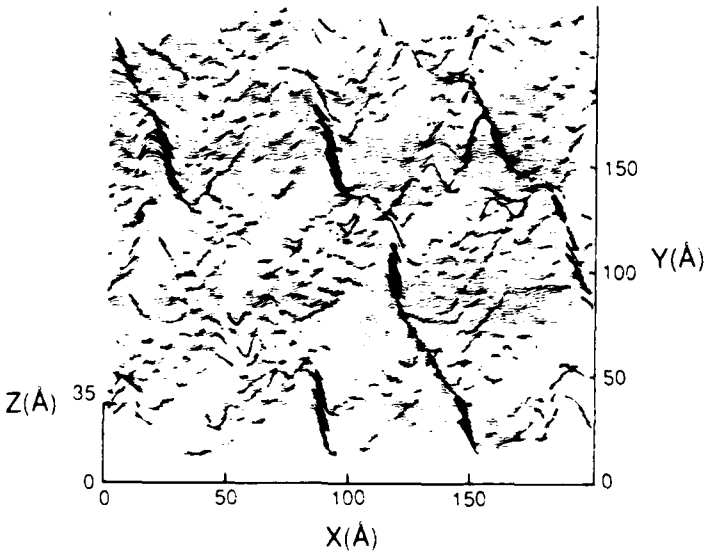

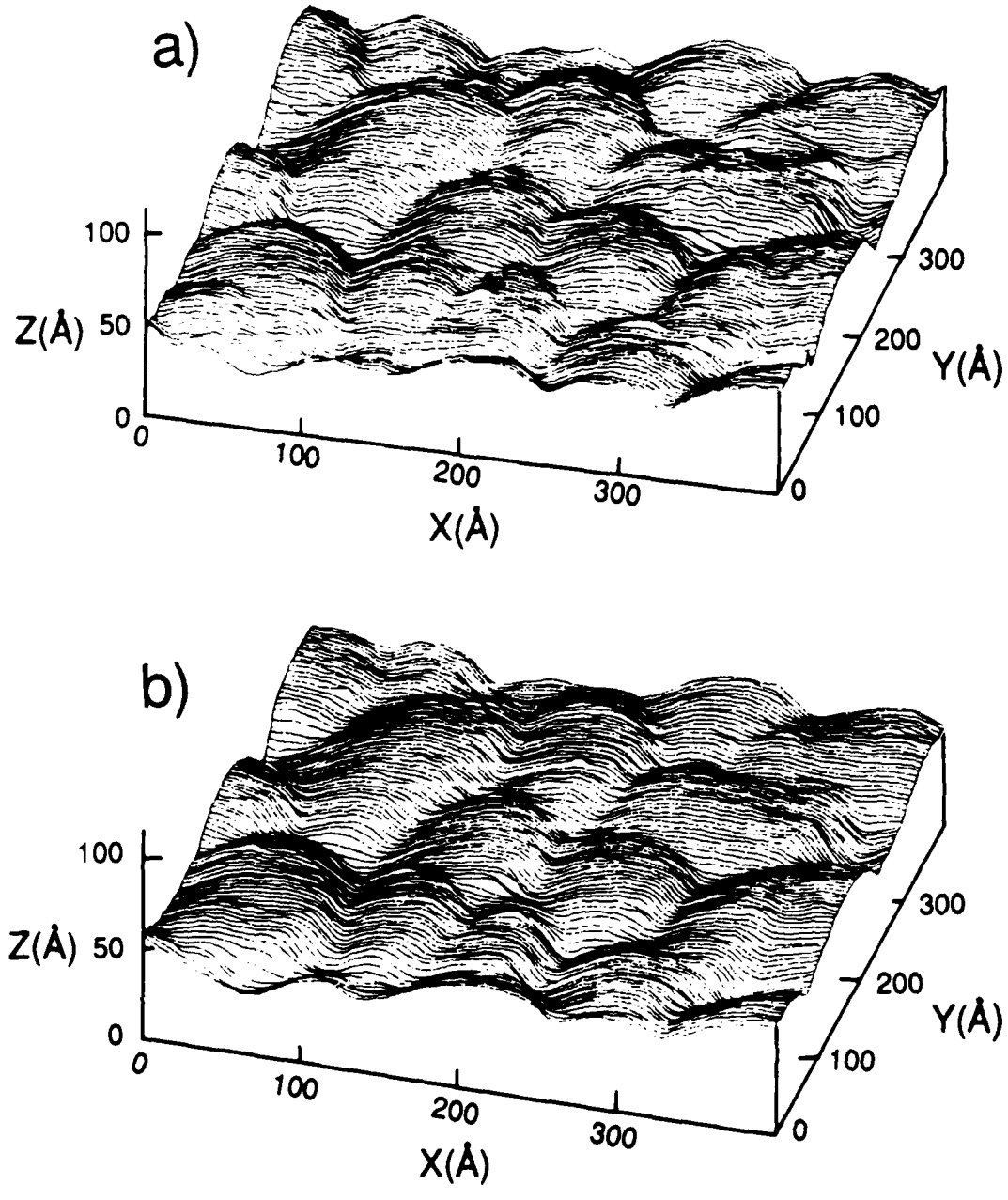
a)
100
Z(Å) 50
0
0
100
200
300
X(Å)
300
200
Y(Å)
100
0
b)
100
Z(Å) 50
0
0
100
200
300
X(Å)
300
200
Y(Å)
100
0

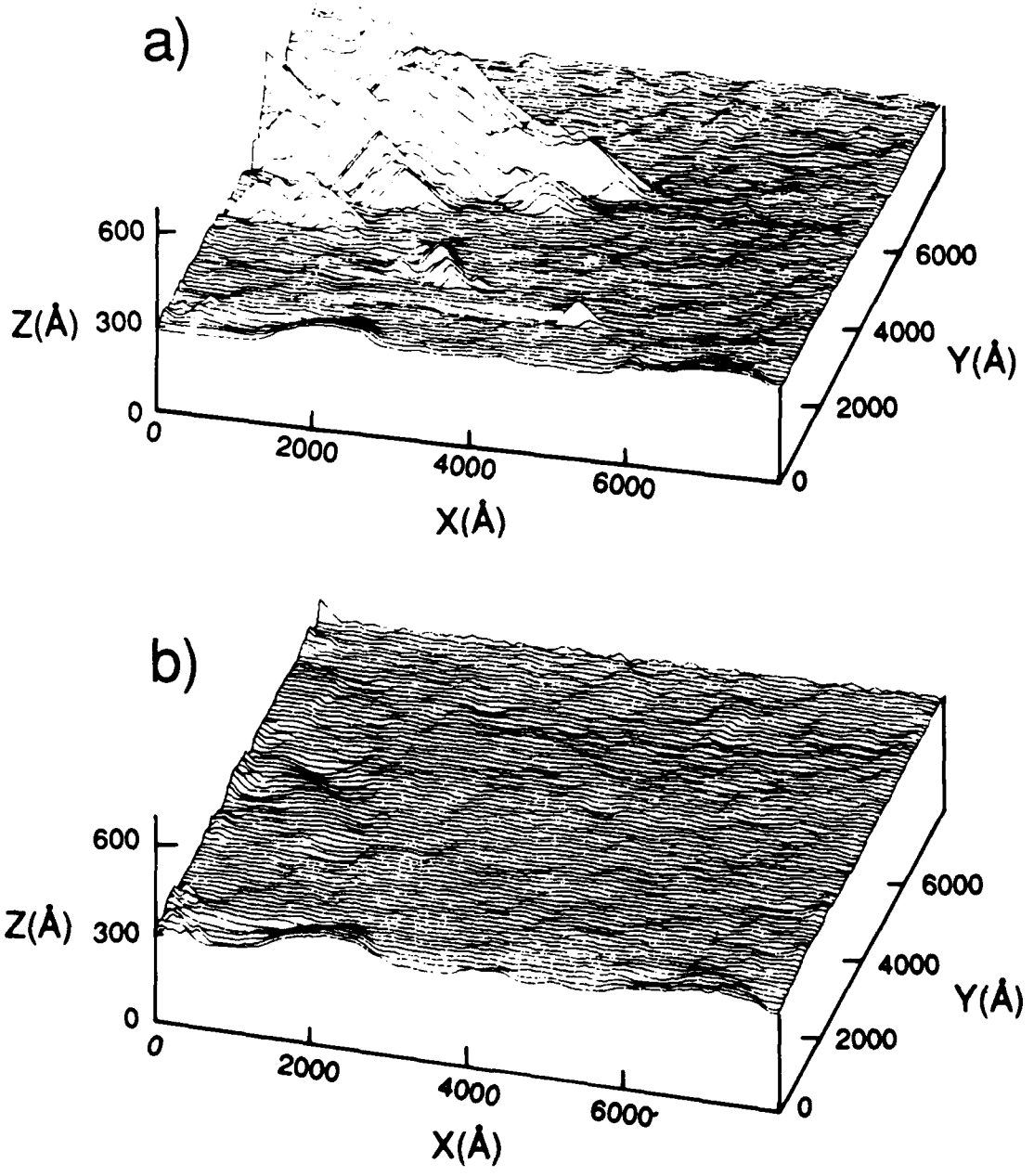
a)
600
Z(Å) 300
0
0
2000
4000
6000
X(Å)
6000
4000
Y(Å)
2000
0
b)
600
Z(Å) 300
0
0
2000
4000
6000
X(Å)
6000
4000
Y(Å)
2000
0

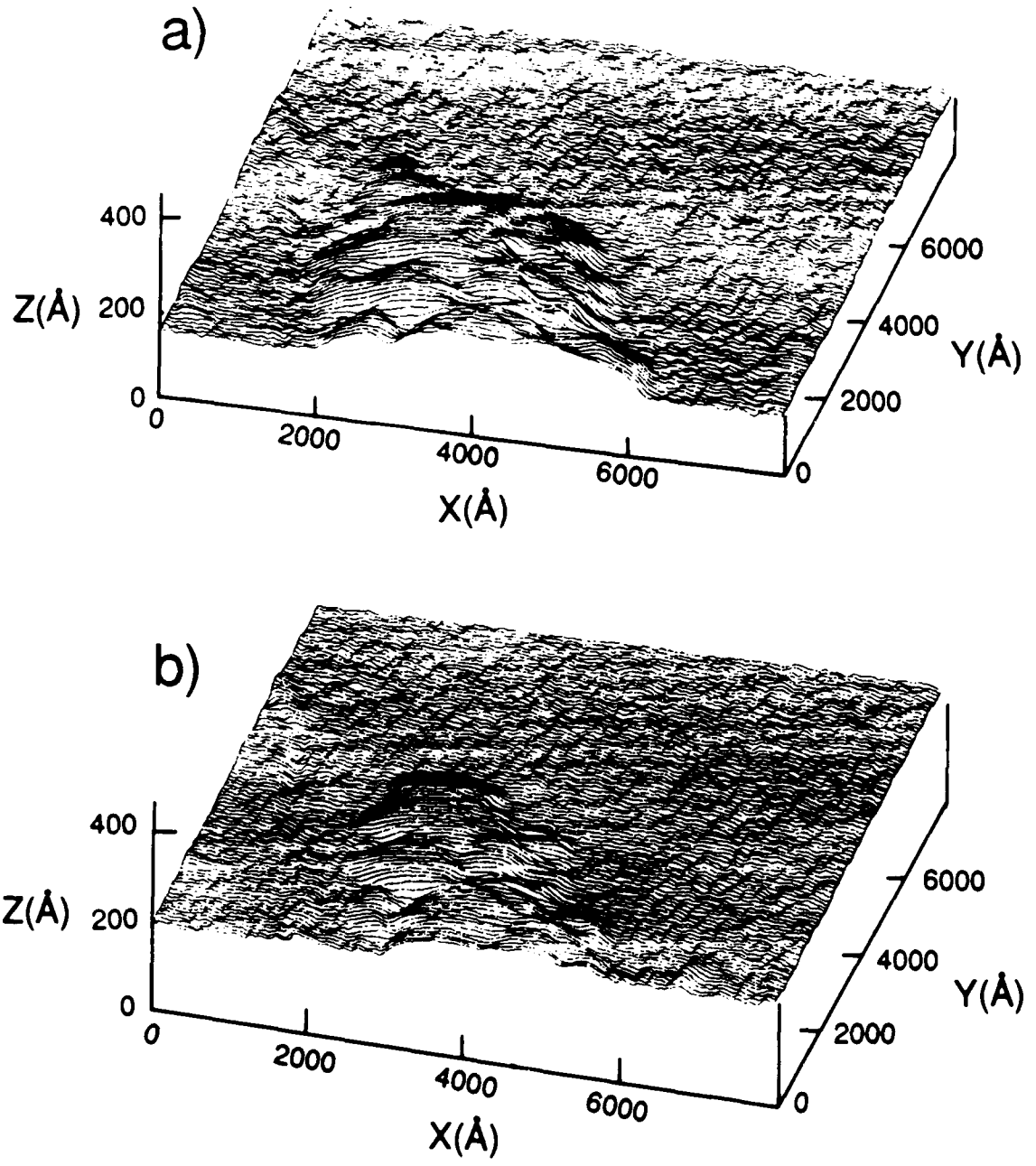
a)
400
200
0
Z(Å)
0
2000
4000
6000
X(Å)
0
2000
4000
6000
Y(Å)
b)
400
200
0
Z(Å)
0
2000
4000
6000
X(Å)
0
2000
4000
6000
Y(Å)